Anisotropy of nonlinear coupling of two counter-propagating waves in photorefractive $Fe:KNbO_3$

G. Cook,[1,2] J. L. Carns,[1,3] M. A. Saleh,[1,4] and D. R. Evans[1,*]
[1]*Air Force Research Laboratory, Materials and Manufacturing Directorate, Wright-Patterson Air Force Base, Ohio 45433, USA*
[2]*Universal Technology Corporation, 1270 N. Fairfield Road, Dayton, Ohio 45432, USA*
[3]*Anteon Corporation, 5100 Springfield Pike, Suite 509, Dayton, Ohio 45431, USA*
[4]*UES, Inc., 4401 Dayton-Xenia Road, Dayton, Ohio 45432, USA*
(Received 4 January 2006; revised manuscript received 23 March 2006; published 1 May 2006)

The dependence of self-pumped photorefractive two-beam coupling in $Fe:KNbO_3$ with crystal angle has been measured at 532 nm for the *a-c* and *b-c* crystal planes using a combination of oil immersion and relay imaging. A significant deviation between existing theory and experiment is found for large crystal angles. We propose this is due to a highly anisotropic effective charge trap density in $Fe:KNbO_3$ of almost two orders of magnitude variation with crystal angle in the *a-c* plane.

DOI: 10.1103/PhysRevB.73.174102 PACS number(s): 61.72.Ss, 42.65.Hw, 42.70.Nq, 71.55.−i

INTRODUCTION

Nonreciprocal light transmission through crystals of iron doped potassium niobate ($Fe:KNbO_3$) occurs by photorefractive beam coupling between two antiparallel beams formed from the incident beam and a Fresnel reflection from the rear of the crystal. Interference between these two counter-propagating beams writes a reflection grating which amplifies one beam and attenuates the other. The direction of amplification depends on the sign of the majority charge carriers, the sign of the electro-optic coefficient, and the crystal orientation.

This phenomenon has been reported in several photorefractive media with the most pronounced effect occurring in iron doped lithium niobate ($Fe:LiNbO_3$) for beam propagation and the grating $\boldsymbol{K}$ vector along the crystal *c* axis in a focal plane geometry.[1–4] Although the electro-optic coefficients in $Fe:KNbO_3$ are generally larger than those of $Fe:LiNbO_3$, nonreciprocal light transmission along the *c* axis in $Fe:KNbO_3$ is less pronounced than with $Fe:LiNbO_3$. This is because $Fe:KNbO_3$ does not have a typically large photovoltaic field which dominates beam coupling in most $Fe:LiNbO_3$ crystals.[5] However, unlike $Fe:LiNbO_3$, for this geometry the effective electro-optic coefficient for $Fe:KNbO_3$ increases dramatically away from the *c* axis for light polarization and grating $\boldsymbol{K}$ vector in the crystal *b-c* plane, reported to reach a maximum at 52.5° from the *c* axis.[6]

Experimentally investigating the crystal angular dependence of self-pumped nonreciprocal light transmission in $Fe:KNbO_3$ is not trivial. Photorefractive $Fe:KNbO_3$ is difficult to grow reproducibly and successive crystals grown using the same apparatus can have a wide variation in beam coupling efficiency. It is also common for individual crystals to have a spatially inhomogeneous photorefractive response.[7] The material is fragile and sensitive to mechanical and thermal stress, making it difficult to retain poling integrity during cutting and polishing operations. Re-poling crystals cut substantially away from the crystal *c* axis is challenging. Our experience suggests that it is difficult to maintain experimental continuity across multiple samples in order to make quantitative measurements. Ideally all comparative angular measurements should be made using a single crystal to avoid the large discontinuities in experimental data reported previously using different crystals.[6] This paper describes the experimental measurement of self-pumped nonreciprocal light transmission through a uniform single crystal of $Fe:KNbO_3$ as a function of the crystal angle with respect to the grating $\boldsymbol{K}$ vector using a combination of oil submersion and relay imaging. Using this technique we show that the optimum crystal angle is substantially smaller than previously reported. We also find the beam coupling with crystal angle deviates significantly from published theory, suggesting the effective charge trap density in $Fe:KNbO_3$ is highly anisotropic. According to our measurements, the effective trap density for the crystal *a-c* plane varies by almost two orders of magnitude with crystal angle.

THEORY

We define the change in transmission due to the presence of a photorefractive grating as being a change in the optical density, ΔOD, given by $\Delta OD = \log_{10}(I_0/I_{PR})$, where I_0 is the linear transmitted intensity prior to the formation of the photorefractive grating and I_{PR} is the steady-state transmitted intensity of the pump beam once the photorefractive grating has formed. Using standard photorefractive theory it is possible to estimate the optical gain coefficient and from this calculate the expected change in ΔOD. Within the photorefractive crystal, standing intensity fringes photoexcite charges which, after being subject to thermal diffusion, result in a steady-state space charge field. Assuming a single majority charge carrier, Kukhtarev's equations lead to the following expression for the space-charge field E_S:[5]

$$E_S = \frac{E_0 + iE_D + E_{PV}}{1 + E_D/E_Q - i[E_0/E_Q + (N_A/N_D)(E_{PV}/E_Q)]} \qquad (1)$$

where E_0 is the bulk electric field, $E_D = 2\pi k_B T/e\Lambda$ is the diffusion field, $E_Q = eN_A/K\epsilon_S$ is the saturation field, E_{PV} is

the photovoltaic field, N_A is the acceptor number density, N_D is the total Fe number density ($Fe^{2+}+Fe^{3+}$), e is the electronic charge, $K=2\pi/\Lambda$ is the spatial frequency in the medium, k_B is Boltzmann's constant, Λ is the grating spacing, T is the absolute temperature, and ϵ_s is the dielectric constant. For $Fe:KNbO_3$ the photovoltaic field is reported to be negligible[8,9] and so, in the absence of an externally applied field, Eq. (1) reduces to

$$E_S = \frac{iE_D}{1+E_D/E_Q}. \tag{2}$$

The intrinsic coupling coefficient, Γ, between the two counter-propagating beams is given by

$$\Gamma = \frac{2\pi}{\lambda} n^3 r_{eff}\,\mathrm{Im}(E_S), \tag{3}$$

where n is the refractive index for a given crystal angle and beam polarization, r_{eff} is the scalar effective electro-optic coefficient, and λ is the wavelength of light in vacuum.

Piezoelectric and photoelastic contributions arising from the space-charge field can significantly affect beam coupling in $Fe:KNbO_3$.[10] The influence of these contributions is described by an effective second rank electro-optic tensor r_{ij}^{eff}, the components of which are given by[10,11]

$$r_{ij}^{eff} = r_{ijk}^{S}\hat{n}_k + p'^{E}_{ijkl}\hat{n}_l A^{-1}_{km} B_m \tag{4}$$

in which

$$A_{ik} = C^{E}_{ijkl}\hat{n}_j\hat{n}_l,$$

$$B_i = e_{kij}\hat{n}_k\hat{n}_j, \tag{5}$$

where r_{ijk}^{S} is the third rank clamped electro-optic tensor, p'^{E}_{ijkl} is the effective fourth rank elasto-optic tensor, C^{E}_{ijkl} is the fourth rank elastic stiffness tensor, e_{kij} is the third rank piezoelectric tensor, and $\hat{n}_{j,k,l}$ is the unit $\boldsymbol{K}$ vector for the space-charge field. Einstein summation over common subscripts applies to these expressions. The scalar electro-optic coefficient is then given by[10]

$$r_{eff} = \hat{n}_P \cdot r_{ij}^{eff} \cdot \hat{n}_S, \tag{6}$$

where $\hat{n}_P$ and $\hat{n}_S$ are the unit vectors for the pump and signal beam polarization vectors, respectively. The piezoelectric and photoelastic effects also influence the dielectric constant, $\epsilon_S = \epsilon_r^{eff}\epsilon_0$, where ϵ_0 is the permittivity of free space and ϵ_r^{eff} is the effective relative dielectric constant given by[11]

$$\epsilon_r^{eff} = \epsilon_{ij}^{S}\hat{n}_i\hat{n}_j + \frac{e_{ijk}e_{mnl}\hat{n}_i\hat{n}_j\hat{n}_m\hat{n}_n A^{-1}_{kl}}{\epsilon_0}, \tag{7}$$

where ϵ_{ij}^{S} is the clamped dielectric tensor.

The saturation field, E_Q, is, therefore, also affected by the piezoelectric and photoelastic effects, as well as by the effective trap density, N_A. The influence this has on beam coupling depends on the relative magnitude of the saturation field with respect to the diffusion field in Eq. (2).

The coupled equations for the counter-propagating beams are[12]

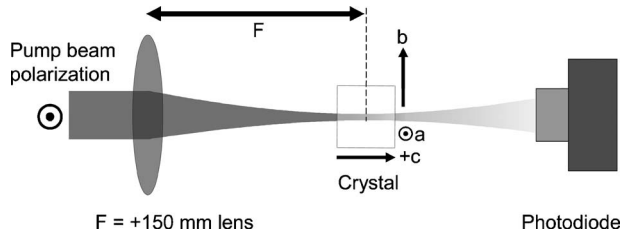

FIG. 1. Method for determining Γ and $I_{Erasure}$ along the crystal c axis.

$$\frac{dI_P}{dz} = -\alpha I_P - \Gamma\frac{I_P I_S}{I_P+I_S+I_{Erasure}} - \frac{2(z-f)I_P}{z_R^2+(z-f)^2}, \tag{8}$$

$$\frac{dI_S}{dz} = +\alpha I_S - \Gamma\frac{I_P I_S}{I_P+I_S+I_{Erasure}} - \frac{2(z-f)I_S}{z_R^2+(z-f)^2}, \tag{9}$$

where I_P is the pump intensity, I_S is the signal intensity, α is the linear absorption coefficient, $z_R=\pi\omega_0^2/\lambda$ is the Rayleigh range for the focusing lens, ω_0 is the $1/e$ spot radius, λ is the pump wavelength, f is the lens focal length, and z is the distance from the beam waist along the beam axis. $I_{Erasure}$ is the equivalent intensity required to erase the grating at the same rate as the sum of contributions from the dark conductivity and any experimentally induced erasure processes such as light scattering from defects, room light, etc.

Equations (8) and (9) can be solved numerically using a shoot and match method with an adaptive Runge-Kutta integration technique to estimate the ΔOD.[3–5] At each iteration, the signal intensity is given by the Fresnel reflection of the pump intensity at the rear of the crystal. Although the specific values of N_A, N_D, and $I_{Erasure}$ are not known for our crystal, Γ and $I_{Erasure}$ can be determined by fitting to measurements of ΔOD along the crystal c axis for a range of input intensities. E_s is then determined by Eq. (3) and we can use this value to calculate the saturation field, E_Q, and the effective trap density, N_A. For a given pump intensity, the values of N_A and $I_{Erasure}$ together with the calculated value of r_{eff} allow Γ and ΔOD to be determined as a function of the crystal orientation.

EXPERIMENT

Γ and $I_{Erasure}$ were determined from measurements of the ΔOD along the crystal c axis using the arrangement shown in Fig. 1. A 5 mm×5 mm×5 mm x-y-z cut crystal of $Fe:KNbO_3$ was carefully selected for its uniform photorefractive properties. Unusually, for $Fe:KNbO_3$, the ΔOD for this crystal was generally invariant across the whole pump face of the crystal, indicating good volumetric uniformity of the photorefractive properties. A 532 nm continuous wave beam from a Coherent Verdi® laser was focused at approximately $f/40$ using a +150 mm focal length plano-convex lens with the beam waist in the middle the $Fe:KNbO_3$ crystal. The beam polarization was parallel to the crystal a axis and beam propagation was along the positive c axis direction. A large area photodiode was used to measure the steady-state transmission for a range of input powers. The

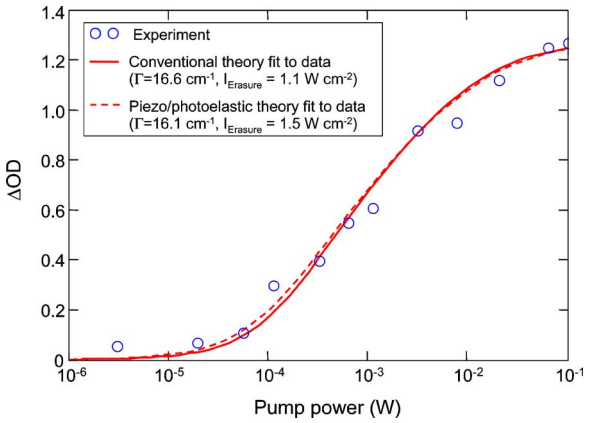

FIG. 2. (Color online) Variation of ΔOD with input power along the *c* axis with best fits for conventional and piezoelectric/photoelastic theories.

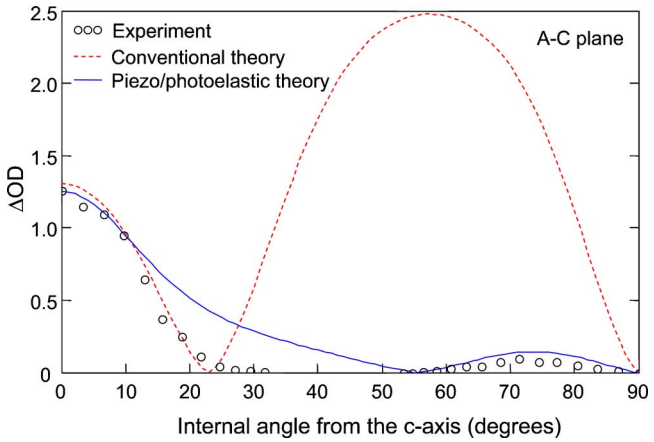

FIG. 4. (Color online) Conventional and piezoelectric/photoelastic theories compared with *a*-*c* plane data.

$Fe:KNbO_3$ crystal had an absorption coefficient of 0.74 cm^{-1} at 532 nm along the crystal *c* axis, polarized parallel to the *a*-*c* plane. The Fe doping concentration in the melt was nominally 1000 ppm. Figure 2 shows the variation in ΔOD with input power for this crystal.

The experimental arrangement for measuring the crystal ΔOD angular dependence is shown in Fig. 3. Three equal focal length lenses formed a relay-imaged optical path through the apparatus with the middle of the crystal placed at the first focus. To allow higher internal beam angles to be accessed, the crystal was submerged under Cargille type "A" immersion oil ($n \approx 1.515$ @ 532 nm) contained within a 20 mm path glass cell. The glass cell was angled away from normal incidence by a few degrees to prevent the rear face of the cell from back reflecting a portion of the pump beam into the focal region in the crystal. Within the glass cell, the crystal was mounted on a low friction neodymium magnet. A complementary magnet was positioned just below the glass cell, fixed to a calibrated rotation stage. Magnetic coupling allowed the crystal to be rotated to any desired angle [owing to the aspect ratio of the crystal and to the refractive index mismatch between the immersion oil and the crystal, internal angles between 32 and 53° with respect to the *c* axis could not be accessed in our experiment]. At the second focus of the relay imaging scheme, a 20% reflectivity mirror generated a counter-propagating signal beam from the transmitted pump. This reflectivity was similar to the ≈16% reflection which occurs at the air interface of bare crystals of $Fe:KNbO_3$. Relay imaging reduced the alignment sensitivity of the rear mirror and ensured a good spatial overlap of the pump and signal beams. This was especially important for internal angles ⩾30° when beam fanning caused significant lateral distortion to the transmitted beam. The experiment was mounted on a vibration isolation table and, as an additional precaution against air currents and acoustic disturbances, the whole experiment was surrounded by foam rubber blocks to stabilize the optical interference fringes within the crystal.

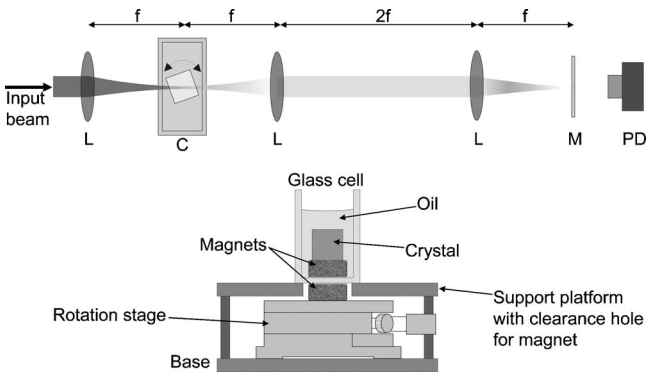

FIG. 3. Optical layout (top) and magnetically coupled crystal rotation stage (bottom). $L=+150$ mm focal length plano convex lenses, C = magnetically coupled oil immersion cell for the crystal, M=20%R mirror, PD=photodiode, $f=150$ mm focal length.

RESULTS AND DISCUSSION

The theoretical fits to the data for the *c*-axis power dependence shown in Fig. 2 give similar gain coefficients of 16.6 and 16.1 cm^{-1} for conventional and piezoelectric/photoelastic theories, respectively, although the piezoelectric theory implies a greater intrinsic erasure intensity ($I_{Erasure}$). Through Eq. (3) the values for these gain coefficients imply space-charge fields with imaginary components of 4.70×10^3 V cm^{-1} and 3.86×10^3 V cm^{-1} for conventional and piezoelectric/photoelastic theory, respectively, leading to values of N_A of 2.1×10^{16} and 5.0×10^{16} cm^{-1} from conventional and piezoelectric/photoelastic theories, respectively. These are comparable with typical published values for $Fe:KNbO_3$ and are assumed to be constants for the material.

Using the above values for N_A, Fig. 4 compares the experimental angular dependence of the ΔOD with conventional and piezoelectric/photoelastic theories for beam propagation and polarization in the crystal *a*-*c* plane. It is clear that in neither case do the theoretical curves properly follow the experimental results. There does seem to be a good correlation between conventional theory and experiment in Fig. 4 for internal angles between zero and 23°, but no correlation exists for larger angles. There is also reasonable agreement between piezoelectric/photoelastic theory and experiment for

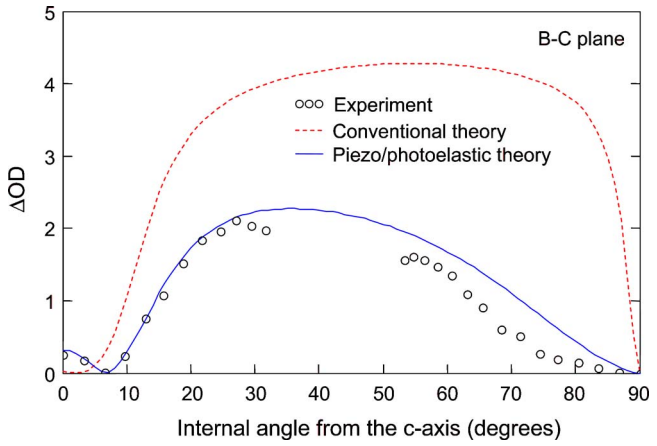

FIG. 5. (Color online) Conventional and piezoelectric/photoelastic theories compared with *b-c* plane data.

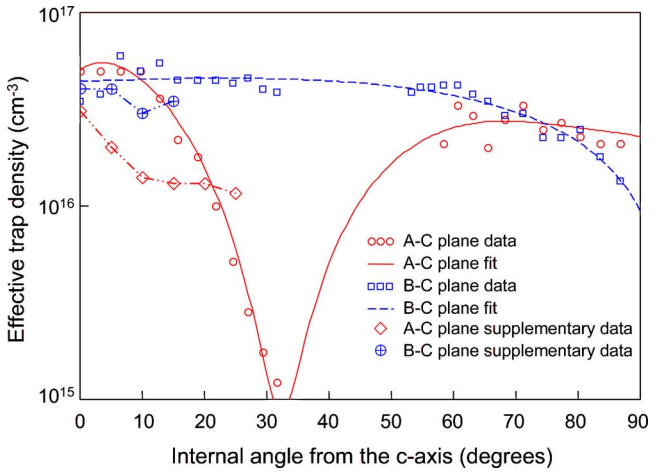

FIG. 6. (Color online) Measured effective trap densities with crystal angle for the *a-c* and *b-c* crystal planes. Supplementary data are from transmission grating measurements.

angles between 55 and 90° from the *c* axis. Note that the gain direction reverses at about 23° for conventional theory and at about 55° for piezoelectric/photoelastic theory. The crystal orientation must be reversed along the *c* axis during the experiment for angles greater than these values. The data presented allow for the reversal of the crystal and absolute values of ΔOD have been plotted in Fig. 4. Confirmation measurements were also taken without reversing the crystal orientation, as a check against orientational error.

Using the same respective values for the space-charge field, Fig. 5 compares the experimental angular dependence of the ΔOD with theory for beam propagation and polarization in the crystal *b-c* plane. For this geometry, conventional theory fails to follow the experimental data. However, piezoelectric/photoelastic theory gives a much closer agreement with experiment, but the agreement is good only at smaller angles and becomes progressively worse at larger angles. Note that the peak beam coupling occurs at a beam propagation angle of approximately 30–35° from the *c* axis, which is considerably smaller than previously published values.[6]

For both the *a-c* and *b-c* crystal planes the piezo/photoelastic theory gives a generally better agreement with experiment than conventional diffusion theory, although the ΔOD (and hence the beam coupling gain) is suppressed compared with theory for beam angles away from the crystal *c* axis. This is particularly apparent in the *a-c* plane for angles between 15 and 35°. A possible reason is that the magnitude of the space charge field is not constant with crystal angle, although this would be surprising in steady state for charge migration dominated by thermal diffusion. This assumption changes if charge migration is also driven by nonthermal mechanisms such as photovoltaic fields. The symmetrical beam fanning observed in our crystal at larger angles does imply the existence of a significant photovoltaic field, in contrast to published literature.[8,9] However, the photovoltaic contribution to the space-charge field is expected to have a cosine dependence with crystal angle which does not account for the observed deviation from theories. Although the presence of a photovoltaic field would adversely affect the grating phase shift [given by the argument of Eq. (1) for the space-charge field], the net gain is always enhanced by the presence of a photovoltaic field, described by Eqs. (1) and (3). This enhancement is greatest in the direction of the photovoltaic field, with a cosine reduction at other angles. To test for the possible influence of the photovoltaic field on beam coupling, the phase shift of the grating with respect to the intensity fringes was measured by mounting the rear 20% reflectivity mirror onto a piezoelectrically driven translator. By translating the rear mirror along the beam path at a rate significantly faster than the response time of the experiment, a transient phase shift could be introduced between the established photorefractive grating and the optical intensity fringes. However, the beam coupling was reduced for all transient phase shifts (both positive and negative phase directions), indicating an ideal 90° phase shift existed in steady state between the index grating and the interference fringes at all crystal angles. The contribution to beam coupling from the photovoltaic effect is, therefore, considered negligible in this experiment and does not account for the deviation of beam coupling from theory at larger angles from the *c* axis.

EFFECTIVE TRAP DENSITY MEASUREMENTS

In an effort to isolate the cause for the theoretical deviation, the measurement procedure used for Fig. 2 to obtain an estimate of the effective trap density, N_A, was repeated using the apparatus shown in Fig. 3 at each measured angle for the *a-c* and *b-c* crystal planes. Assuming the published values[10,11] for the electro-optic, elasto-optic, elastic stiffness and piezoelectric tensors are correct, Fig. 6 shows the derived apparent effective trap density as a function of crystal angle for both crystal planes. There is a surprising marked variation of the effective trap density with crystal angle in both cases, but the apparent *a-c* plane effective trap density variation is particularly pronounced, changing by almost two orders of magnitude with crystal angle. Fitted empirical functions used to describe the effective trap density variations with crystal angle for the *a-c* and *b-c* planes, respectively, are

$$N_{A(AC)} = -9.09 \times 10^{12}\theta^6 + 3.03 \times 10^{15}\theta^5 - 3.85 \times 10^{17}\theta^4 + 2.26 \times 10^{19}\theta^3 - 5.67 \times 10^{20}\theta^2 + 3.21 \times 10^{21}\theta + 5 \times 10^{22}, \quad (10)$$

$$N_{A(BC)} = -6 \times 10^{16}\theta^3 + 1 \times 10^{20}\theta + 4.42 \times 10^{22}, \quad (11)$$

where $N_{A(AC,BC)}$ are the effective trap densities in units of m^{-3} for the *a*-*c* and *b*-*c* crystal planes, respectively, and θ is the beam propagation angle in degrees with respect to the crystal *c* axis.

We have also considered the existence of anisotropic gratings arising from angular variations of the absorption coefficient and photoexcitation cross section.[13–15] However, the variations in absorption coefficient appear to be insufficient to account for our observations [$\alpha = 0.72\ cm^{-1}$ (along the *a*-axis) to $0.74\ cm^{-1}$ (along the *c* axis) for the *a*-*c* plane, polarized parallel to the *a*-*c* plane]. We have additionally considered anisotropic gratings arising from any anisotropy of the charge diffusion constants with crystal angle. This would certainly affect the transient response of the crystal but should not influence the steady state results upon which our calculations are based.

Competition between electrons and holes can lead to a reduction in gain,[16–18] and any crystal angular dependence of the electron and hole diffusion coefficients could lead to an angular variation of beam coupling. However, our crystals do not display any change in the sign of the optical gain coefficient with grating spacing, a key indicator of the presence of electron-hole competition.[19] The photorefractive gratings in our experiment decay with a single time constant, indicating a single majority charge species is present. Furthermore, competition between electrons and holes should reduce the net beam coupling in steady state, whereas the observed strong beam coupling supports the presence of a single charge species. For these reasons any competition between electrons and holes is thought to be an unlikely reason for the angular discrepancies between theory and experiment. Although surprising, anisotropy of the effective trap density is therefore the most likely cause of the deviation from previously published theories.

We have made a concerted effort to independently verify the unprecedented variation in the effective trap density using the standard method of measuring the small signal gain as a function of the grating spacing using a combination of transmission and reflection grating measurements.[19] The method relies on identifying the optimum grating spacing to determine the effective trap density of the material. By repeating these measurements over a range of crystal angles, the effective trap density as a function of the crystal angle and crystal plane can be obtained. Owing to the tensoral nature of the electro-optical, piezoelectric, and photoelastic coefficients, it is not possible to obtain an analytic expression for the optimum grating spacing for each crystal angle. Our approach has, therefore, been to adjust the scalar effective trap density for each given crystal angle until the theoretical optimum grating spacing coincides with the experimental observations for that crystal angle. By repeating this process for each crystal angle and crystal plane, the effective trap density can be extracted as a function of the crystal orientation.

This method, although simple in concept, is experimentally extremely challenging in our situation. As the crystal is rotated, the relative angles of incidence of the pump and signal beams become asymmetrical, leading to rotation of the grating $\boldsymbol{K}$ vector with respect to the crystal axes. The mechanical angle of the crystal, therefore, required adjustment for every change of the beam intersection angles in order to maintain a constant grating $\boldsymbol{K}$-vector orientation. It was also very important to maintain a good spatial overlap between the pump and signal beams for all beam intersection angles and crystal orientations. This demanded making the pump beam larger in diameter than the signal beam. The relatively large diameter of the pump beam made it necessary to rotate the crystal towards the pump in order to avoid clipping of the pump beam by the crystal edges. The large diameter pump beam and large gain coefficients promoted excessive competition between signal amplification and parasitic photorefractive coupling arising from scattered pump light, leading to strong beam fanning and spurious beams. It proved impossible to make meaningful measurements at crystal angles beyond 25° in the *a*-*c* plane or 15° in the *b*-*c* plane. We attempted to reduce the overall gain using an external incoherent light source to compete with the grating formation, but this was ineffective and we could not prevent competition from parasitic photorefractive processes. These are the primary reasons we used the method shown in Fig. 2 to obtain trap density information, which we believe to be more reliable than the results obtained from the transmission grating method described above. However, the transmission grating trap density measurements did show qualitative agreement with our reflection grating observations. The transmission grating results are shown as supplementary data in Fig. 6. There is clear evidence that the *b*-*c* plane effective trap density remains approximately constant with crystal orientation, whereas the *a*-*c* plane effective trap density apparently falls sharply as the grating $\boldsymbol{K}$ vector is rotated away from the crystal *c* axis, supporting our earlier observations from self-pumped reflection gratings.

The effective trap density data from Fig. 6 (reflection grating values) can be used to produce a revised theoretical estimate of the ΔOD with crystal angle by using the fitted empirical functions for the effective trap density variations for the *a*-*c* plane [Eq. (10)] and for the *b*-*c* plane [Eq. (11)] in place of the previously fixed value of N_A. Using this approach, Fig. 7 shows the calculated ΔOD for both crystal planes and gives strong agreement with experiment. Note that the trap density data was obtained from a different experiment and data set than the original ΔOD measurements, so that the good agreement between theory and experiment is not due to a circular argument from using common data.

The apparent presence of an anisotropic trap density is rather surprising and has important implications for semiconductors in general, not just photorefractive materials. An implausible explanation is that the trap sites are somehow sensitive to the polarization state of the original photon used to excite the electron (or hole) into the conduction (or valence) band. Each charge would need to retain information about the original exciting photon. It is widely assumed that this information is lost once an electron becomes delocalized in

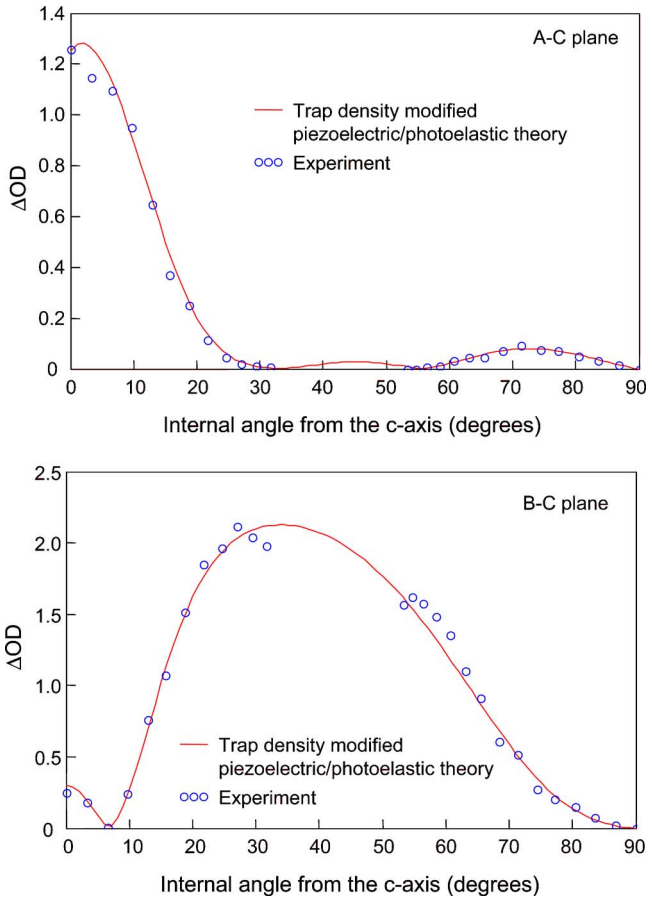

FIG. 7. (Color online) ΔOD variation with crystal angle using the angular effective trap density measurements for the *a-c* and *b-c* crystal planes.

the conduction band. If information of the original exciting photon is not lost, as has been assumed, then this could account for the observed trap density anisotropy. However, we believe this to be unlikely because the electron spin relaxation times are orders of magnitude faster than the electron trapping times.

As an alternative explanation for the apparent anisotropy, we propose that the effective trap sites within $KNbO_3$ may occupy a complex "layered" structure. Growth of $KNbO_3$ does not occur smoothly with a constant growth rate and instead proceeds in a stochastic manner adding a plethora of microscopically thin layers of new material to the existing bulk single crystal. It has been observed that impurities tend to segregate at the boundaries between these structures.[20] It is reasonable to assume that the added impurities (Fe) form a stratified concentration of traps (Fe^{3+} and intrinsic defects) at these boundaries. If the mean distance between adjacent layers varies with crystal angle, the effective trap density could become highly anisotropic when the mean layer separation becomes comparable to, or greater than, the optical fringe separation. For gratings with $\boldsymbol{K}$ vectors predominantly parallel to the layers, the average trap density would appear approximately constant. Whereas for gratings with $\boldsymbol{K}$ vectors generally orthogonal to the layers, some fringes would experience very low effective trap densities while others would have higher trap densities. For this situation, the local space-charge field may saturate in the low trap density regions, leading to an overall reduction in beam coupling. We note, however, that the proposed layering of the trap structure must be irregular in nature; a regular spatial frequency would lead to an intrinsic trap grating in the crystal, leading to competition with the photorefractive grating when the respective $\boldsymbol{K}$ vectors become parallel. An intrinsic trap grating should be observable using incoherent light, but we did not find any such gratings in our crystal.

CONCLUSIONS

The dependence of self-pumped photorefractive two-beam coupling in $Fe:KNbO_3$ with crystal angle has been characterized for the *a-c* and *b-c* crystal planes at 532 nm. Existing piezoelectric/photoelastic theory gives better agreement with experiment than conventional diffusion theory, but significant deviations occur at large angles from the *c* axis, especially for the *a-c* crystal plane. We find evidence to suggest that the effective charge trap density in $Fe:KNbO_3$ may be highly anisotropic with almost two orders of magnitude variation with crystal angle in the *a-c* plane, leading to a tensoral, rather than scalar, description of the effective trap density in $Fe:KNbO_3$. We propose that the apparent trap density anisotropy could be due to a concentration of traps at the interface between adjacent irregular growth layers during crystal production.

ACKNOWLEDGMENTS

We gratefully acknowledge useful discussions with John Seim, Sergei Basun, Ivan Biaggio, Roger Reeves, G. Frank Imbusch, Richard Sutherland, and Scott Holmstrom.

*Corresponding author: dean.evans@wpafb.af.mil

[1] I. F. Kanev, Sov. Phys. JETP **47**, 834 (1978).
[2] Z. Krumins, Z. Chen, and T. Shiosaki, Opt. Commun. **117**, 147 (1995).
[3] G. Cook, C. J. Finnan, and D. C. Jones, Appl. Phys. B **68**, 911 (1999).
[4] D. C. Jones and G. Cook, Opt. Commun. **180**, 391 (2000).
[5] G. Cook, J. P. Duignan, and D. C. Jones, Opt. Commun. **192**, 393 (2001).
[6] M. Z. Zha and P. Günter, Opt. Lett. **10**, 184 (1985).
[7] P. Amrhein and P. Günter, OSA Photonic Science Topical Meeting Ser. 14, AD-A253 001, 166 (1991).
[8] P. Günter and F. Micheron, Ferroelectrics **18**, 27 (1978).
[9] A. E. Krumins and P. Günter, Phys. Status Solidi A **55**, 185 (1979).
[10] M. Zgonik, K. Nakagawa, and P. Günter, J. Opt. Soc. Am. B **12**,

1416 (1995).
[11] M. Zgonik, R. Schlesser, I. Biaggio, E. Voit, J. Tscherry, and P. Günter, J. Appl. Phys. **74**, 1287 (1993).
[12] G. Cook, D. C. Jones, C. J. Finnan, L. L. Taylor, and A. W. Vere, Proc. SPIE **3798**, 2 (1999).
[13] G. Montemezzani and M. Zgonik, Phys. Rev. E **55**, 1035 (1997).
[14] G. Montemezzani, Phys. Rev. A **62**, 053803 (2000).
[15] J. Castillo-Torres, J. A. Hernandez, C. P. Medrano, E. G. Camarillo, and H. S. Murrieta, Opt. Mater. **22**, 251 (2003).
[16] F. P. Strohkendl, J. M. C. Jonathan, and R. W. Hellwarth, Opt. Lett. **11**, 312 (1986).
[17] M. B. Klein and G. C. Valley, J. Appl. Phys. **57**, 4901 (1985).
[18] C. Medrano, E. Voit, P. Amrhein, and P. Günter, J. Appl. Phys. **64**, 4668 (1988).
[19] L. Solymar, D. J. Webb, and A. Grunnet-Jepsen, *The Physics and Applications of Photorefractive Materials* (Clarendon, Oxford, 1996).
[20] M. B. Mishra and S. G. Ingle, J. Appl. Phys. **45**, 5152 (1974).